21. W. C. Nierman et al., Proc. Natl. Acad. Sci. U.S.A. **98**, 4136 (2001).
22. S. G. Andersson et al., Nature **396**, 133 (1998).
23. H. Ogata et al., Science **293**, 2093 (2001).
24. At a late phase of this project, we became aware of an independent effort to sequence the *A. tumefaciens* C58 genome. The work of these authors is published jointly in this issue [D. Wood et al., Science **294**, 2317 (2001)]. The two independently derived sequences are in excellent overall agreement, with single nucleotide discrepancies far below current accuracy standards (99.99%) for finished sequence. Our sequence contains two small insertions relative to that of Wood et al.; one each in the circular chromosome and pAtC58. Further work will determine which of the observed discrepancies reflect strain differences and which reflect errors.
25. M. L. Boschiroli, V. Foulongne, D. O'Callaghan, Curr. Opin. Microbiol. **4**, 58 (2001).
26. K. L. Karem, C. D. Paddock, R. L. Regnery, Microbes Infect. **2**, 1193 (2000).
27. Supplementary Web material is available on Science Online at www.sciencemag.org/cgi/content/full/294/5550/2323/DC1.
28. DNA sequence and protein predictions are available at the National Center for Biotechnology Information's Entréz Genomes Server (www.ncbi.nlm.nih.gov/PMGifs/Genomes/micr.html). The GenBank accession numbers are NC_003062 (circular chromosome), NC_003063 (linear chromosome), NC_003064 (pAtC58) and NC_003065 (pTiC58).
29. A. K. Brassinga, R. Siam, G. T. Marczynski, J. Bacteriol. **183**, 1824 (2001).
30. P. L. Li, S. K. Farrand, J. Bacteriol. **182**, 179 (2000).
31. T. M. Finan et al., Proc. Natl. Acad. Sci. U.S.A. **98**, 9889 (2001).
32. E. Moreno, FEMS Microbiol. Rev. **22**, 255 (1998).
33. J. F. Heidelberg et al., Nature **406**, 477 (2000).
34. R. L. Tatusov, Nucleic Acids Res. **29**, 22 (2001).
35. S. Karlin, Trends Microbiol. **9**, 335 (2001).
36. J. Deneke, G. Ziegelin, R. Lurz, E. Lanka, Proc. Natl. Acad. Sci. U.S.A. **97**, 7721 (2000).
37. S. Casjens et al., Mol. Microbiol. **26**, 581 (1997).
38. L. S. Kahng, L. Shapiro, J. Bacteriol. **183**, 3065 (2001). Kahng and Shapiro analyzed the appearance of hemimethylated DNA, upon passage of a replication fork, at the *att* locus in *A. tumefaciens*. At the time of their study, *att* was believed to reside on the circular chromosome, but we correctly locate it on pAtC58. Thus, at least one *repABC* origin, and probably all three, is coordinated with the cell cycle.
39. K. Skarstad (personal communication) has shown by flow cytometry that all DNA replication is restricted to a relatively short time span within the cell cycle of *A. tumefaciens*.
40. I. J. Domian, A. Reisenauer, L. Shapiro, Proc. Natl. Acad. Sci. U.S.A. **96**, 6648 (1999).
41. Z. Kelman, M. O'Donnell, Annu. Rev. Biochem. **64**, 171 (1995).
42. D. Capela et al., Proc. Natl. Acad. Sci. U.S.A. **98**, 9877 (2001).
43. M. J. Barnett et al., Proc. Natl. Acad. Sci. U.S.A. **98**, 9883 (2001).
44. A. Schluter, S. Ruberg, M. Kramer, S. Weidner, U. B. Priefer, Mol. Gen. Genet. **247**, 206 (1995).
45. L. Otten et al., Mol. Plant Microbe Interact. **5**, 279 (1992).
46. M. J. Bessman, D. N. Frick, S. F. O'Handley, J. Biol. Chem. **271**, 25059 (1996).
47. G. V. Plano, J. B. Day, F. Ferracci, Mol. Microbiol. **40**, 284 (2001).
48. C. H. Shaw, Bioessays **13**, 25 (1991).
49. G. M. Young, D. H. Schmiel, V. L. Miller, Proc. Natl. Acad. Sci. U.S.A. **96**, 6456 (1999).
50. E. M. Lai, O. Chesnokova, L. M. Banta, C. I. Kado, J. Bacteriol. **182**, 3705 (2000).
51. M. Van Montagu, J. Schell, in *Plasmids of Medical, Environmental & Commercial Importance*, K. M. Timmis, A. Puhler, Eds. (Elsevier, Amsterdam, 1979), pp. 71–95.
52. I. R. Henderson, F. Navarro-Garcia, J. P. Nataro, Trends Microbiol. **6**, 370 (1998).
53. K. LeVier, R. W. Phillips, V. K. Grippe, R. M. Roop 2nd, G. C. Walker, Science **287**, 2492 (2000).
54. M. Purcell, H. A. Shuman, Infect. Immun. **66**, 2245 (1998).
55. R. Penyalver, P. Oger, M. M. Lopez, S. K. Farrand, Appl. Environ. Microbiol. **67**, 654 (2001).
56. M. Krishnan, J. W. Burgner, W. S. Chilton, S. B. Gelvin, J. Bacteriol. **173**, 903 (1991).
57. G. LaPointe, C. S. Nautiyal, W. S. Chilton, S. K. Farrand, P. Dion, J. Bacteriol. **174**, 2631 (1992).
58. S. M. Lyi, S. Jafri, S. C. Winans, Mol. Microbiol. **31**, 339 (1999).
59. L. B. Willis, G. C. Walker, J. Bacteriol. **181**, 4176 (1999).
60. P. L. Schuerman, J. S. Liu, H. Mou, A. M. Dandekar, Appl. Microbiol. Biotechnol. **47**, 560 (1997).
61. T. K. Bhat, B. Singh, O. P. Sharma, Biodegradation **9**, 43 (1998).
62. S. Subramaniyan, P. Prema, FEMS Microbiol. Lett. **183**, 1 (2000).
63. D. Parke, J. Bacteriol. **177**, 3808 (1995).
64. R. D. Vierstra, S. J. Davis, Semin. Cell Dev. Biol. **11**, 511 (2000).
65. Supported by funds from Cereon Genomics; Monsanto Company; the University of Richmond; and the National Institutes of Health, National Institute of General Medicine (grant R15 GM61690-01 to B.W.G.). We thank the University of Richmond students of the 1999 and 2000 genetics course and the 2000 and 2001 microbiology course for assistance; S. Salzberg, C. Frasier, and The Institute for Genome Research for providing GLIMMER; and L. S. Kahng, J. Elhai, R. Last, J. Hirschberg, A. Matthysse, S. Winans, S. Farrand, and the manuscript's reviewers for helpful discussions, well-reasoned criticisms, and corrections to our original annotations.

3 October 2001; accepted 19 November 2001

Earthquake Recurrence and Rupture Dynamics of Himalayan Frontal Thrust, India

Senthil Kumar,[1]* Steven G. Wesnousky,[1] Thomas K. Rockwell,[2] Daniel Ragona,[2] Vikram C. Thakur,[3] Gordon G. Seitz[4]

The Black Mango fault is a structural discontinuity that transforms motion between two segments of the active Himalayan Frontal Thrust (HFT) in northwestern India. The Black Mango fault displays evidence of two large surface rupture earthquakes during the past 650 years, subsequent to 1294 A.D. and 1423 A.D., and possibly another rupture at about 260 A.D. Displacement during the last two earthquakes was at minimum 4.6 meters and 2.4 to 4.0 meters, respectively, and possibly larger for the 260 A.D. event. Abandoned terraces of the adjacent Markanda River record uplift due to slip on the underlying HFT of 4.8 ± 0.9 millimeters per year or greater since the mid-Holocene. The uplift rate is equivalent to rates of fault slip and crustal shortening of $9.6^{+7.0}_{-3.5}$ millimeters per year and $8.4^{+7.3}_{-3.6}$ millimeters per year, respectively, when it is assumed that the HFT dips 30° ± 10°.

The ongoing collision of India into Eurasia has produced four major thrust earthquakes along the ~2500-km length of the Himalayan front during the past ~100 years (*1*), yet none of the events reportedly produced coseismic surface ruptures (*2*, *3*) (Fig. 1A). Here, we report paleoseismological evidence of the size and timing of surface-rupturing thrust earthquakes along the HFT as well as a quantitative bound on the rate of fault slip on the HFT, from a site located about 80 km northwest of Dehra Dun.

Regional setting. The collision of India with Eurasia since the Eocene has accommodated 2000 to 3000 km of convergence (*4*). The boundary between the Indian and Eurasian plates forms an arc that extends ~2500 km across the continent (Fig. 1A). Plate motion models and recent Global Positioning System (GPS) measurements indicate that convergence between the Indian and Eurasian plates is between about 40 and 50 mm/year (*5*, *6*). Between about 10 and 20 mm/year of the total 40 to 50 mm/year of convergence is taken up by thrust motion along the Himalayan arc, with the remainder taken up farther to the north by a combination of thrusting, crustal extension, and strike-slip motion within the Eurasian Plate (*3*, *7*–*9*). Three major south-verging thrust faults strike the length of the Himalayan arc (Fig. 1). The northernmost of the three thrusts is the Main Central Thrust (MCT), which emerges along the southern edge of the High Himalaya and has not been observed to break Quaternary deposits and, hence, is generally considered inactive (*10*). The Main Boundary Thrust (MBT) marks the southern edge of the Lesser Himalaya, is expressed in bedrock along the arc, and is locally observed to displace Quaternary deposits (*10*, *11*). The southernmost thrust is the HFT, which is now considered to be the most active of the three and delineates the northern limit of the exposed Indian Plate.

[1]Center for Neotectonic Studies, University of Nevada, Reno, NV 89557, USA. [2]Department of Geological Sciences, San Diego State University, San Diego, CA 92182, USA. [3]Wadia Institute of Himalayan Geology, 33, G. M. Singh Road, Dehra Dun 248001, UP, India. [4]Lawrence Livermore National Laboratory, Livermore, CA 94551, USA.

*To whom correspondence should be addressed. E-mail: senthil@seismo.unr.edu

The HFT displaces Tertiary and Quaternary sediments of the Siwalik Group over the Indo-Gangetic plain (*11*) (Fig. 1).

The region of most severe shaking and damage associated with the major historical earthquakes along the Himalayan arc is generally bounded by the MCT to the north and the HFT to the south (*1*) (Fig. 1A). Instrumentally recorded seismicity of moderate magnitude events is concentrated beneath the MCT at depths between about 10 and 20 km (*12*) (Fig. 1B). Active deformation along the HFT is expressed by scarps, uplift, and folding of late Quaternary and Holocene deposits (*10*, *11*). The largest earthquakes have been interpreted to occur along a shallowly dipping décollement that extends beneath the Lesser and Sub-Himalayas and emerges as the HFT (Fig. 1) (*1*). It remains today somewhat of a conundrum that geological evidence of late Quaternary surface rupture is visible along the HFT, yet none of the major historical earthquakes have reportedly produced surface rupture (*2*, *3*).

Structural setting. The Black Mango tear fault is located along the northwestern portion of the HFT between two areas of intense shaking associated with the magnitude (M_s) ~7.8 1905 earthquake (*13*) (Fig. 1). The fault transforms motion between two segments of the HFT and passes through the small town of Kala Amb (Fig. 2) (*14*). Scarps in Quaternary alluvium are not distinct along the main trace of the HFT near Kala Amb. Displacement on the underlying HFT has produced an asymmetric south-verging anticline within the Siwalik Group in the hanging wall (Fig. 3). Near Kala Amb, Siwalik beds on the back limb of the anticline show northerly dips ranging between 20° and 40°. Dip directions reverse and are as steep as 60° to the south on the forelimb of the anticline (*15*). Similar structures are observed elsewhere along the HFT and have been attributed to fault-bend or fault-propagation folding (*8*). Uplift observed on the east side of the Black Mango fault is due to displacement on the underlying and dipping HFT (Fig. 2). The dip of the underlying HFT beneath the back limb of the fold is equal to or greater than the dip of strata in the back limb (30° ± 10°), depending on the presence or absence of internal shear in the hanging wall (*16*).

Longer term uplift along the HFT is reflected in fluvial strath terraces of the Markanda River, which are abruptly truncated by the Black Mango fault and now sit about 27 m above the active stream grade (*14*). The terraces occur as thin remnants along the Black Mango fault and as broad well-preserved flats along the Markanda River (*14*). The strath deposits rest on Siwalik bedrock, are generally about 7 m thick where not eroded, consist of rounded pebble-cobble gravels, and are commonly capped by 1 to 2 m of fine-grained loamy sand. Radiometric dates on two fragments of charcoal collected from a finer grained lens 4.7 m below the terrace surface provide a maximum age of the terrace surface: 4896 ± 68 and 5069 ± 205 calendar years before present (cal years B.P.), respectively (Table 1). Abandonment of the Markanda terrace is attributed to tectonic uplift on the basis of the truncation of the terraces by the Black Mango fault. Dividing the 27-m relative uplift of the terraces by the younger detrital charcoal date yields a minimum bound on the uplift rate of 4.8 ± 0.9 mm/year. If we assume that the dip of the HFT beneath the Siwalik hills is 30° ± 10°N and that the uplift of the terraces reflects displacement on the underlying HFT, the rate of slip on the HFT is limited to $9.6^{+7.0}_{-3.5}$ mm/year. The equivalent rate of horizontal contraction for these fault dips and slip rate is $8.4^{+7.3}_{-3.6}$ mm/year.

Earthquake displacement and recurrence. We excavated a trench across a scarp of the Black Mango fault expressed in younger alluvium to place bounds on the size and recurrence time of the most recent of the earthquakes that have produced uplift of the Markanda terraces (Fig. 4). The trench is located near the village of Kheri Taprion, where the fault curves and joins with the HFT. Vertical separation between the hanging and footwall surfaces of the well-expressed scarp at the trench site is ~4.8 m. The ~55-m-long trench exposure shows that the scarp is principally the result of slip and folding associated with four low-angle thrusts, labeled F1, F2, F3, and F4 in Fig. 4.

Sheared and faulted packages of Siwalik-derived colluvium and weathered bedrock units on the hanging wall above fault strand F1 are the oldest in the exposure and labeled unit 1 in Fig. 4. The intensity of shearing within these hanging wall units indicates that the hanging wall has been deformed by several earthquakes. No scarps are associated with the shears within the Siwalik colluvium and bedrock that reach the surface, although the overlying soil is

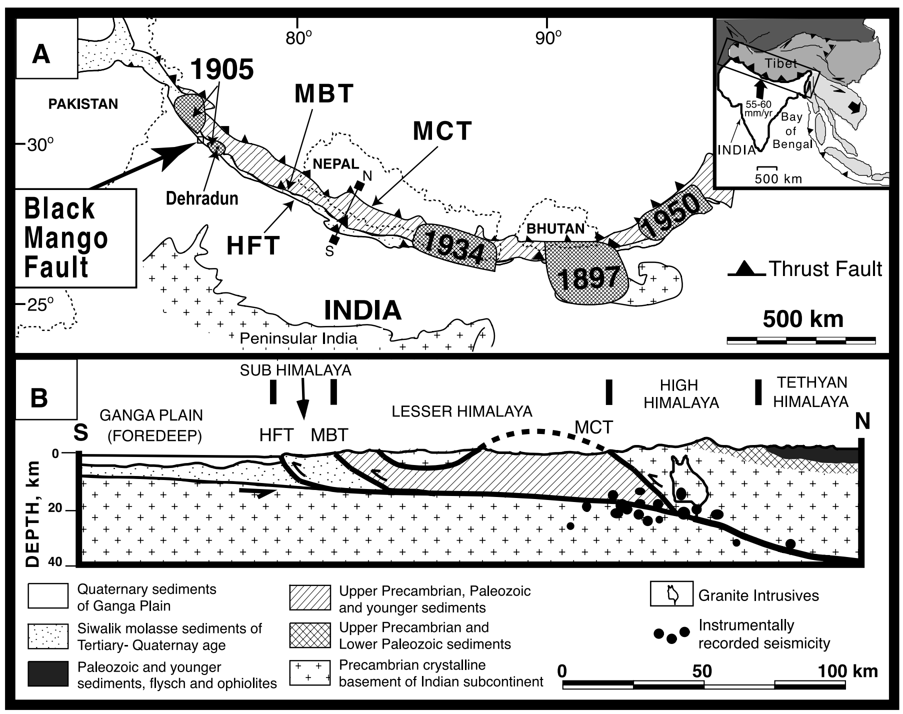

Fig. 1. (**A**) Major thrust faults and meizoseismal zones (shaded and labeled with date) of major historical earthquakes along the ~2500-km-long Himalayan arc (*1*) and location of the Black Mango fault. Major thrust faults are the Main Central Thrust (MCT), the Main Boundary Thrust (MBT), and the Himalayan Frontal Thrust (HFT) (*11*). (**B**) Generalized north-south geologic section across the Himalaya for the central portion of the Himalayan arc. Location of the cross section is indicated on (A) by small squares connected by line (*1*).

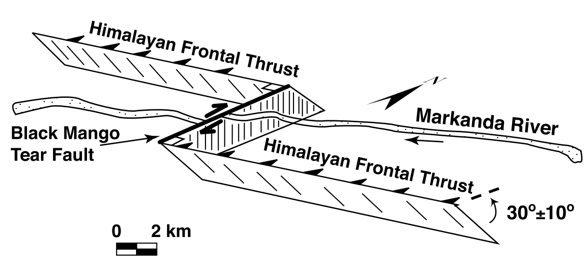

Fig. 2. The Black Mango fault transforms motion between two main thrust segments of the HFT. Teeth on hanging wall of thrusts and half-sided arrows show relative strike slip along Black Mango fault.

stripped and the accommodation of strike-slip motion on these shears is likely. The unconformity between the fan gravel units (unit 2) to the southwest and the Siwalik materials on the hanging wall is a scarp, probably tectonic in origin and predating deposition of fan gravel units. The now buried scarp may reflect displacement on trace F4 observed only at the very base of the trench. The fan gravel unit includes two distinct facies: coarser channel fill deposits of pebble-cobble size clasts with few boulders (unit 2a) and intervening massive fine and medium silty sand (unit 2b). The fan gravel unit dips 14° southwestward in the exposure and is displaced by fault strands F1, F2, and F3. The southwesternmost flat-lying beds on the footwall (unit 3) are a sequence of younger medium to fine silty sand and pebbly fine sand that contain two distinct buried soil horizons, Qb1 and Qb2, respectively.

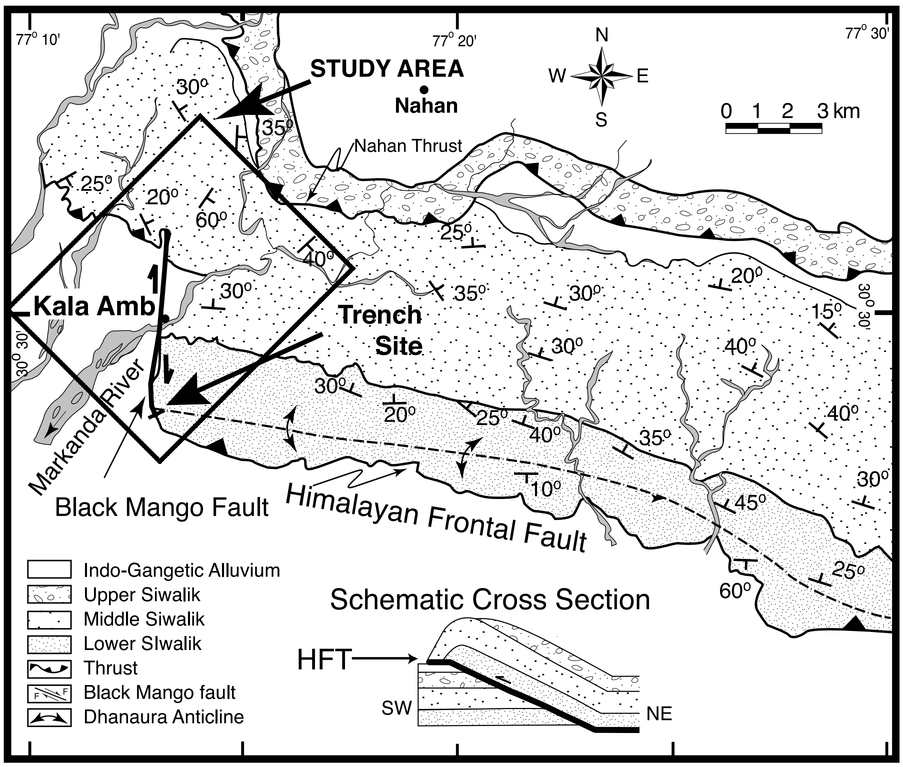

Fig. 3. Geology and schematic cross section of Kala Amb area shows location of Black Mango fault (*12*). Box outlines portion of the area examined during this study.

Fault strand F3 cuts the lower soil Qb1 but not the upper Qb2 soil. The soil Qb1 on the footwall is interpreted to have been at the ground surface, perhaps buried by a thin veneer of younger sediment, at the time of displacement of fault strand F3. Displacement on F3 resulted in shearing of soil horizon Qb1 and ploughing of sediments now preserved immediately beneath the upward termination of the F3 strand. A sequence of radiocarbon dates on detrital charcoal immediately beneath Qb1 places the maximum age of the Qb1 surface and, hence, displacement on F3, at 1349 ± 55 A.D. (sample C-18 in Fig. 4 and Table 1). Displacement on F3 was followed by continued accumulation and onlap of the fine-grained sands of unit 3 on the footwall and development of soil Qb2. The uppermost portion of unit 2b on which Qb2 soil is developed is probably scarp-derived colluvium composed of unit 2b materials. Fault strand F2 cuts higher in the section and disrupts sediment at the level of the Qb2 soil horizon. Cross-cutting relationships were not sufficient to uniquely determine whether F2 disturbs sediments of unit 3 above soil Qb2. A colluvial layer from which a radiocarbon sample (C-24) yielded a modern age is the oldest unit unambiguously not disturbed by F2. The age of detrital charcoal recovered from soil horizon Qb2 (sample C-15 in Fig. 4 and Table 1) places a maximum bound on the age of the F2 displacement at 1523 ± 99 A.D. Strand F1 reaches within a meter of the surface and probably occurred coeval with displacement on F2 but may also have slipped earlier with F3. In sum, displacements on fault traces F1, F2, and F3 are interpreted to be the result of two earthquakes having occurred during the past 600 years, between 1349 ± 55 A.D. and 1523 ± 99 A.D. and after 1523 ± 99 A.D.

The amount of slip in each earthquake is not

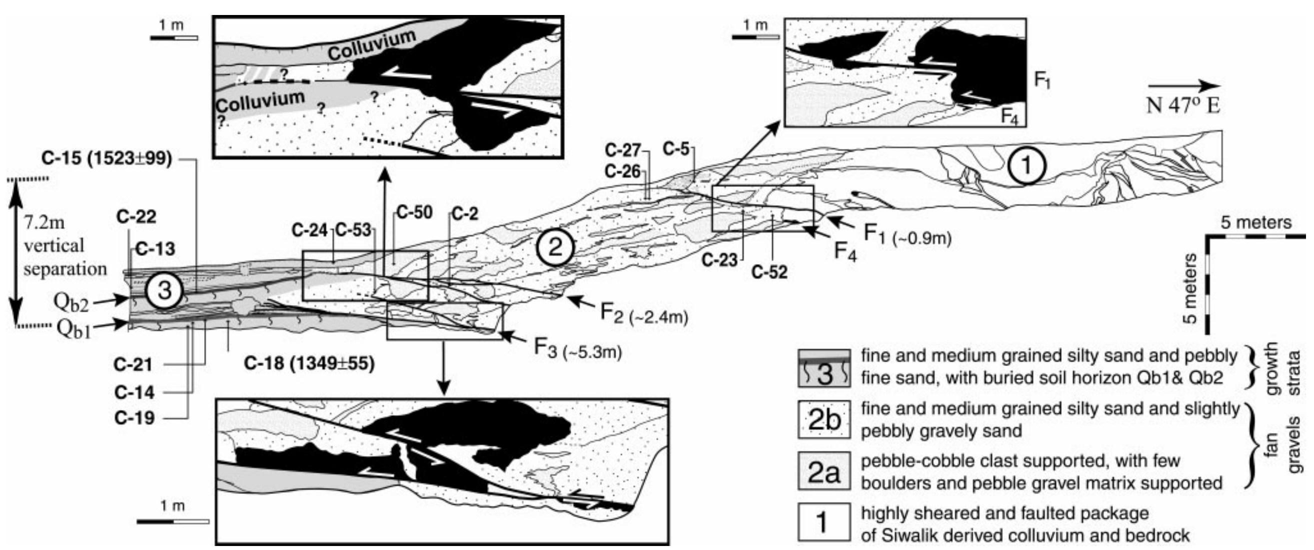

Fig. 4. Map of trench wall showing fault traces (bold), amount of offsets (parentheses, in meters), and radiocarbon sample locations and labels. Dendrochronologically corrected calendar age ranges in years B.C./A.D. are shown for sample C-18 and C-15. Locations of discrete displacements on traces F1, F2, and F3 are enlarged in insets. The units used to measure fault offset are shaded black in the insets.

uniquely determined. Total displacement during the two events is 8.6 m, with 0.9, 2.4, and 5.3 m recorded on strands F1, F2, and F3, respectively (Fig. 4). We may attribute the 5.3 m of slip on F3 to the 1349 ± 55 A.D. event and the 2.4 m of slip on F2 to the 1523 ± 99 A.D. event. Slip of 0.9 m recorded on F1 is probably due to the 1523 ± 99 A.D. event, in which case slip during the 1349 ± 55 A.D. event was about 1.5 times that for the 1523 ± 99 A.D. event. Up to 0.7 m of slip on F3 is possibly due to slip during the latter 1523 ± 99 A.D. event, in which case the discrepancy in slip is not as great.

Vertical separation of the surface represented by the buried soil Qb1 and hanging wall surface of the present-day scarp is 7.2 m (Fig. 4). Restoration of displacements on the shallow dipping F1, F2, and F3 strands only accounts for 1 m of the 7.2 m vertical separation. There are two reasons for this discrepancy. First, the scarp reflects folding in addition to fault displacement, in which case the fault displacements recorded by F1, F2, and F3 are minimum measures of fault displacement for the earthquakes. Second, there existed a scarp before the occurrence of the two earthquakes that produced slip on F1, F2, and F3. The displacement responsible for the preexisting scarp is recorded by the steeply dipping unconformable contact between the Siwalik materials on the hanging wall (unit 1) and the fan gravels (unit 2) that now dip about 14° southwest. The scarp may be the result of displacement on fault strand F4, a shear at the base of the Siwaliks sediments exposed in the hanging wall. Strict interpretation of radiometric ages shows the dip panel of fan gravels to have been emplaced in between about 38 B.C. and 775 A.D. Sample C-23 is interpreted to be reworked detrital charcoal on the basis of its older age as compared with samples C-2 and C-52 from the same stratigraphic level. On that basis, we infer that deposition of the gravels occurred in yet a briefer period of time between 261 and 775 A.D. and further speculate that the pulse of sedimentation across the scarp reflects deposition after a single earthquake that occurred at about 261 A.D. The exposed thickness of sediments in the dip panel provides a minimum bound on the vertical displacement (4 m) across the scarp formed during the hypothesized 261 A.D event. If the vertical displacement is due to slip on shallow dips of 9° to 12° observed for faults F1, F2, and F3, then this event was larger than the subsequent events.

Major historical thrust earthquakes have not been observed to produce surface ruptures, so the observation of surface rupture along the Black Mango fault leads to interesting questions concerning the mechanics of earthquakes along the HFT. Modern-day seismicity along the HFT is concentrated at depths between about 10 and 20 km below the MCT (*12*) (Fig. 1). Similarly, available GPS studies indicate that modern-day strain accumulation is concentrated above the MCT and nearly absent to the south between the MCT and HFT, where the meizoseismals of the great historical thrusts are located (*7*). These observations indicate that the major historical earthquakes initiated at a point of localized strain accumulation beneath the MCT and propagated southward on the order of 100 km along a shallow décollement that surfaces as the HFT (*1*). Given that none of the major historical earthquakes have reportedly produced surface rupture, the observations from the Black Mango trench suggest at least three possible interpretations. First, the earthquakes recorded in the trench represent lesser, although certainly large, displacements localized on the toe of an essentially flat and very shallow décollement surface of the HFT. Alternatively, they reflect earthquakes that initiate at the MCT that are large enough to propagate to the surface at the HFT and, in that sense, yet larger than the major earthquakes that have already been recorded historically. Finally, there exists a possibility that none of the major historical earthquakes occurred on the HFT, as suggested recently for the 1897 earthquake of Assam (*17*). Another puzzle arises when considering that the Black Mango fault lies between the two distinct meizoseismal regions of the 1905 earthquake (*18*, *19*) (Fig. 1). Historical reports (*18*) and reanalyses (*19*) of the 1905 event report no evidence of surface rupture. However, within the resolution of our measurements, the incomplete historical reports, and the observed youthfulness of the scarp and associated fractures, it is possible that the 1905 Kangra earthquake is recorded as the younger slip event in our trench.

Table 1. Radiocarbon analyses of charcoal samples from trench (see Fig. 4 for sample location).

Location	Sample no. and Laboratory no.*	$\delta^{13}C$	^{14}C age† (1σ)	Calendar age range‡ in calender years A.D./B.C.) (2σ)
		Trench samples		
Unit 3	C-24 (71081)	−28.2	Modern	Modern
Unit 3	C-22 (71079)	−25.3	230 ± 40	1530–1947 A.D.
Unit 3 (Qb2)	C-15 (71076)	−25.1	420 ± 40	1423–1519, 1593–1622 A.D.
Unit 3	C-13 (71075)	−11.4	650 ± 40	1281–1402 A.D.
Unit 3 (Qb1)	C-18 (72127)	−25.8	620 ± 30	1294–1405 A.D.
Unit 3	C-21 (71078)	−25	680 ± 50	1262–1399 A.D.
Unit 3	C-14 (72126)	−25.6	920 ± 30	1021–1217 A.D.
Unit 3	C-19 (72128)	−26.7	940 ± 40	1017–1211 A.D.
Unit 2	C-53 (77315)	−25	1390 ± 70	539–775 A.D.
Unit 2	C-26 (71082)	−24.6	1420 ± 40	559–673 A.D.
Unit 2	C-50 (77313)	−25	1450 ± 50	535–665 A.D.
Unit 2	C-27 (71083)	−24.5	1470 ± 40	534–657 A.D.
Unit 2	C-5 (71074)	−24.1	1520 ± 40	429–639 A.D.
Unit 2	C-2 (71073)	−24	1600 ± 40	385–558 A.D.
Unit 2	C-52 (77314)	−25	1630 ± 50	261–541 A.D.
Unit 2	C-23 (71080)	−25	1900 ± 60	38 B.C. to 243 A.D.
		Terrace samples		
Terrace	MT001-5 (77316)	−25	4300 ± 40	3015–2878 B.C.
Terrace	MT001-3 (73705)	−28.4	4410 ± 40	3325–2915 B.C.

*CAMS; Center for Accelerator Mass Spectrometry, Lawrence Livermore National Laboratory. †Reported ^{14}C ages use Libby's half-life (5568 years). Delta ^{13}C values are assumed when given without decimal places. ‡Dendrochronologically calibrated age ranges were calculated with the University of Washington calibration program Calib 4.2, using the intercepts method (*20*), and age ranges are often discontinuous. Discrete intervals provided only for Qb1 and Qb2.

References and Notes

1. L. Seeber, J. Armbruster, in *Earthquake Prediction: An International Review, Maurice Ewing Series*, vol. 4 (American Geophysical Union, Washington, DC, 1981), pp. 259–277.
2. R. S. Yeats, V. C. Thakur, *Curr. Sci.* **74**, 230 (1998).
3. S. G. Wesnousky, S. Kumar, R. Mohindra, V. C. Thakur, *Tectonics* **18**, 967 (1999).
4. P. Molnar, P. Tapponnier, *Sci. Am.* **236**, 30 (April 1977).
5. C. De Mets, R. Gordon, D. Argus, S. Stein, *Geophys. Res. Lett.* **21**, 2191 (1994).
6. J. Paul *et al.*, *Geophys. Res. Lett.* **28**, 647 (2001).
7. R. Bilham, *Nature* **386**, 61 (1997).
8. P. M. Powers, R. J. Lillie, R. S. Yeats, *Geol. Soc. Am. Bull.* **110**, 1010 (1998).
9. J. Lave, J. P. Avouac, *J. Geophys. Res.* **105**, 5735 (2000).
10. T. Nakata, *Geol. Soc. Am. Spec. Pap.* **232**, 243 (1989).
11. ———, *Sci. Re. Tohoku Univ. 7th Ser.* **22**, 39 (1972).
12. J. Ni, M. Barazangi, *J. Geophys. Res.* **89**, 1147 (1984).
13. N. Ambraseys, R. Bilham, *Curr. Sci.* **79**, 45 (2000).
14. Supplementary material is available at www.sciencemag.org/cgi/content/full/294/5550/2328/DC1
15. J. P. Srivastava, S. N. Verma, V. K. Joshi, B. C. Verma, R. K. Arora, in *GSI Proceedings Neogene/Quaternary Boundary Field Conference, India, 1979* (Geological Survey of India, India, 1981), pp. 233–241.
16. J. Suppe, C. D. Connors, Y. Zhang, in *Thrust Tectonics*, *AAPG Mem.*, in press.
17. R. Bilham, *Nature* **410**, 806 (2001).
18. C. S. Middlemiss, *Mem. Geol. Surv. India* **38**, 405 (1910).
19. R. Bilham, *Geophys. J. Int.* **144**, 713 (2001).
20. M. Stuiver *et al.*, *Radiocarbon* **40**, 1041 (1998).

21. This research is supported by NSF grant EAR 9972955. This is CNS contribution 39. We thank R. Bürgmann and J. Suppe for insightful comments on an early draft of this manuscript and the three anonymous reviewers for constructive suggestions. This work was performed under the auspices of the U.S. Department of Energy by University of California Lawrence Livermore National Laboratory under contract W-7405-Eng-48.

12 September 2001; accepted 7 November 2001